Chapter 2
Instrumentation for FUV Spectroscopy

Akifumi Ikehata, Yusuke Morisawa, and Noboru Higashi

Abstract This chapter describes recent breakthroughs in the instrumentation for far-ultraviolet (FUV) spectroscopy. The key technique is attenuated total reflection (ATR) that is frequently used in the infrared region. ATR technique decreases the absorbance of samples with strong absorptivity because of the penetration depth of the evanescent wave less than 100 nm. Therefore, ATR–FUV spectroscopy realizes the measurement of FUV spectra of samples in liquid and solid states. Some applications (in-line monitoring, characterization of polymers and time-resolved spectroscopy in sub-microsecond) are introduced in terms of instrumentation. This chapter explains not only the detail of the instruments but also the mathematical correction for ATR spectra to separate the absorption and refraction indices.

Keywords Attenuated total reflection (ATR) • Internal reflection element • Kramers–Kronig transformation • Time-resolved ATR–FUV spectroscopy

2.1 Introduction

FUV spectra give considerable information, but the absorption intensities are so strong particularly for liquids and solids that the light cannot penetrate even in a thin film. Therefore, FUV spectroscopy had been exclusively used for the measurement of gas. The use of FUV spectroscopy for liquids and solids was very limited for the regular reflection from the surface of the sample with troublesome operations. As an effective technique to obtain spectra of materials with strong absorption, attenuated

A. Ikehata (✉)
National Food Research Institute, National Agriculture and Food Research Organization, (NARO), 2-1-12 Kannondai, Tsukuba, Ibaraki 305-8642, Japan
e-mail: ikehata@affrc.go.jp

Y. Morisawa
Department of Chemistry, School of Science and Engineering, Kinki University, 3-4-1 Kowakae, Higashi-Osaka, Osaka 577-8502, Japan

N. Higashi
Kurabo Industries Ltd., 14-5 Shimokida-cho, Neyagawa, Osaka 572-0823, Japan
e-mail: Noboru_Higashi@ad.kurabo.co.jp

Y. Ozaki, S. Kawata (eds.), *Far- and Deep-Ultraviolet Spectroscopy*,
DOI 10.1007/978-4-431-55549-0_2

total reflection infrared (ATR-IR) spectroscopy with an internal reflection element (IRE) has been widely used [1–3]. Since the penetration depth of the evanescent wave, defined as the distance required for the electric field amplitude to fall e^{-1} of its value from the surface of the IRE [4], is less than the wavelength, the ATR method allows the spectral measurement similar to that of transmittance spectra with a very short optical path length. Thus, the ATR method provides benefits both in terms of quantitative measurements and easy handling of liquid or solid samples with strong absorption, compared to transmittance spectroscopy. Despite the fact that ATR techniques have been modified in a multitude of ways to obtain IR [3, 5, 6], near IR [7, 8], and UV-visible spectra [9–12], there were no ATR methods for the FUV region before 2007. ATR–FUV spectroscopy opened the way for the measurement of the dense materials with strong absorptivities [13].

Recently the time-resolved ATR–FUV spectrometer was developed for the study of radical species in chain reaction to measure the transient absorption spectra of stable and radical species based on ATR [14]. In order to investigate a chemical reaction, in particular a chain reaction, both the product and the reactant should be observed. Typical reactants, that is to say generally stable species, do not show absorption spectra in the UV–VIS region but do so in the FUV region. Moreover, by setting the observation region to be at a higher energy than that of the excitation laser light that induces photochemical reactions, we have been able to avoid the effects of fluorescence on our spectroscopic observations.

The former part of this chapter describes the technical problems of ATR measurement in the FUV region, and the latter part explains an expanded application of ATR–FUV spectroscopy to the detection of transient phenomena in aqueous solutions.

2.2 Attenuated Total Reflection Spectroscopy in FUV Region

Higashi and coworkers designed and constructed an ATR-based FUV spectrometer [15]. In this spectrometer the design of a small internal reflection element (IRE) probe has led to successful measurement of the entire $\tilde{A} \leftarrow \tilde{X}$ transition absorption band of water and aqueous solutions.

Figure 2.1 shows a schematic diagram of this instrument [15]. Figure 2.1a depicts a portionof the custom design of a commercial FUV spectrometer (KV-200, Bunko-Keiki, Tokyo, Japan). Figure 2.1b illustrates a flow cell unit formed between the sapphire IRE probe (7) and a fluorinated resin holder (8) enlarged from the area marked with a dashed line (part b) in Fig. 2.1a. The probe is fixed in place by the holder made by PTFE (8), with the flow sample cell formed by a space between the PTFE guide (9) and the aperture (1) of the probe. A liquid sample for measurement is drawn into the 2-mm-diameter aperture in the IRE probe. Air in the sealed instrument is purged with pure nitrogen gas. To control the sample temperature over the range of 5–80 °C, a Peltier element (10) is in contact with the probe holder (8) by a heat pipe (11).

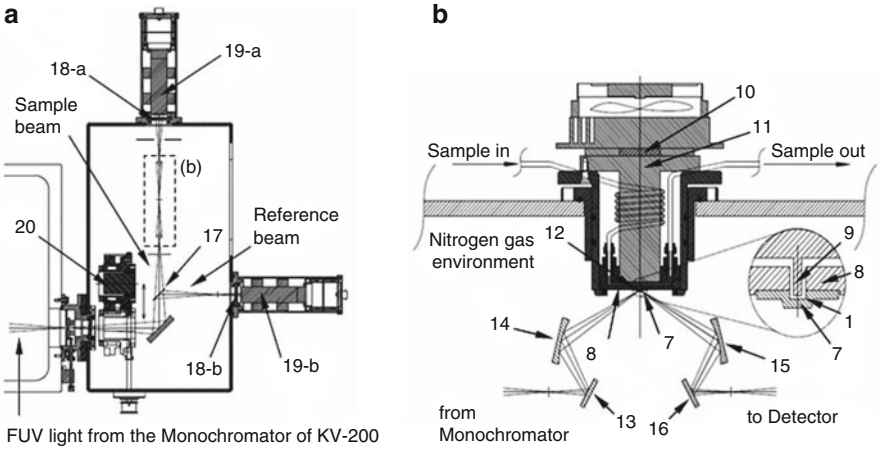

Fig. 2.1 Schematic diagram of the ATR–FUV spectrometer. (**a**) Originally designed semi-double beam part for the commercial KV-200 spectrometer. (**b**) The ATR probe with temperature control system

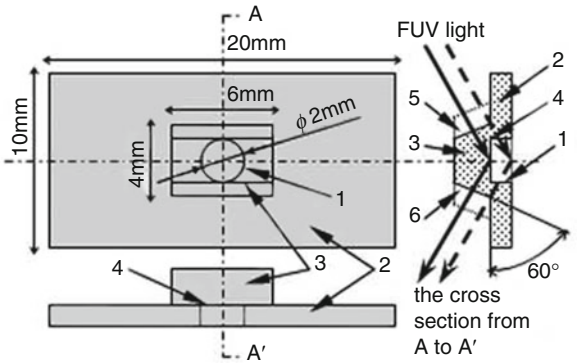

Fig. 2.2 Description of the ATR probe. It consists of a trapezoidal internal reflection element (IRE) and a rectangular base plate with a cylindrical aperture

A 30-W deuterium lamp was used as the light source for the KV-200 spectrometer, which incorporated a diffraction grating with 2,400 grooves/mm and a blazed wavelength of 150 nm. As depicted in Fig. 2.1a, the FUV light from the monochromator is split into a reference beam and a sample beam by an MgF_2 beam splitter. The reflected light and the reference beam finally pass through a synthetic quartz plate coated with sodium salicylic acid, which fluoresces. Fluorescence of each beam is then detected by a photomultiplier.

Figure 2.2 depicts the developed IRE probe [15]. The IRE used with the ATR technique must satisfy following two important conditions. One is that the refractive index of the IRE must be greater than that of the sample material, and another is that the IRE material must have sufficient transmission in the measured wavelength range. For the full FUV region (120–200 nm), there seemed no ideal IRE material that fulfills both conditions. Materials such as sapphire with a higher refractive index

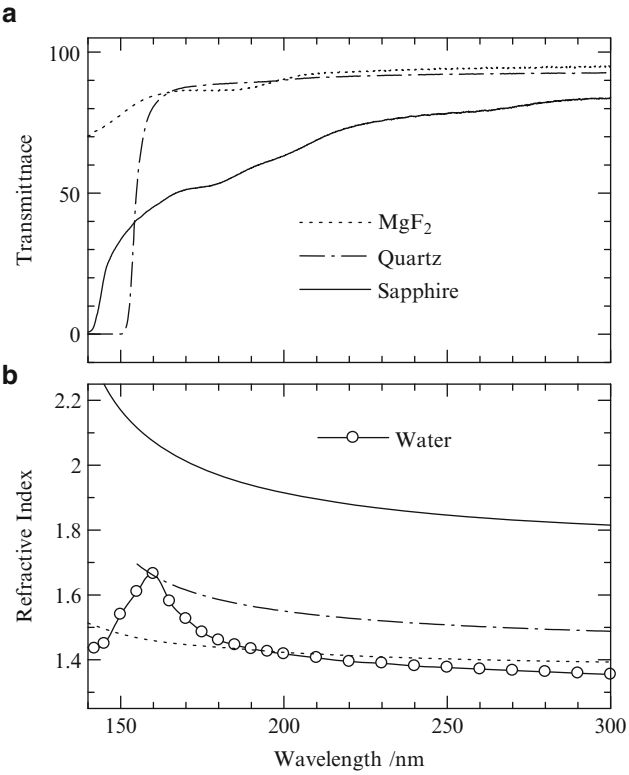

Fig. 2.3 Transmittance (**a**) and refractive indices (**b**) of materials in the FUV–UV region

than water have insufficient transmission, while those with sufficient transmission (e.g., MgF_2, CaF_2, and synthetic quartz) have lower refractive indices than water in the FUV region (see Fig. 2.3). Although sapphire lacks sufficient transmission in the wavelength region shorter than 145 nm, the property of the high refractive indices is suitable for the IRE for FUV spectroscopy. Higashi et al. therefore used sapphire for the IRE with a single reflection and an angle of incidence of 60°.

The ATR probe consists of two parts: a trapezoidal IRE and a rectangular base plate with a cylindrical aperture (1) as shown in Fig. 2.2. These two parts are integrated by an optical contact technique. Adhesives are not used to prevent sample contamination and residue from remaining in the device. The base plate sits on the same side of the IRE at which it comes into contact with the sample through the aperture at the interface surface (4). The IRE itself has both an incident surface (5) and an outgoing surface (6), which are not in contact with the sample. FUV light entering the incident surface perpendicularly strikes the incident interface surface and then perpendicularly exits the outgoing surface. For the ATR instrument, any

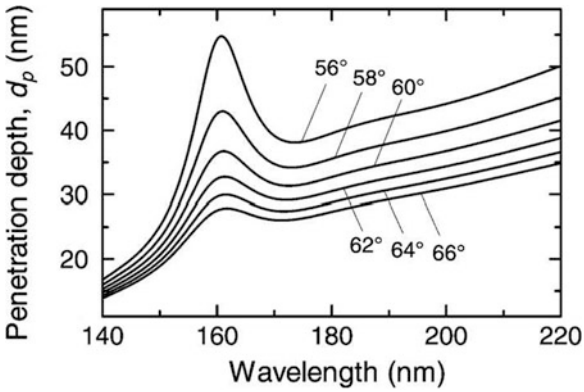

Fig. 2.4 Simulated penetration depth of the evanescent wave in water for incident angles over the range of 56°–66° by Eq. (2.1)

kind of liquids can be used as the sample. Solid samples can also be investigated but good contact between the IRE and a solid sample is required.

The penetration depth of the evanescent wave d_p is dependent on the ratio of the refractive indices of the IRE, n_1, and sample, n_2, as follows: [16]

$$d_p = \frac{\lambda}{2\pi n_1 \sqrt{\sin^2\theta - (n_2/n_1)^2}} \tag{2.1}$$

Figure 2.4 shows simulated results of penetration depth of the evanescent wave in water from sapphire IRE in different incident angles over the range of 56°–66°. For the calculation, reported refractive indices of water [17] and sapphire [18] were substituted into Eq. (2.1). A marked increase of the penetration depth happens at around 161 nm as shown in Fig. 2.4, as the refractive index of water has a maximum value over 1.65 between normal and anomalous dispersions at 159 nm (see Fig. 2.5a) [15]. The dash-dot line in Fig. 2.5a represents refractive index and the solid line depicts the absorption index of water. The refractive index n and the absorption index k have distinct maxima at 159 and 151 nm, respectively. Figure 2.5b shows the calculated (broken lines) and measured (solid lines) ATR–FUV spectra at a variety of incident angles. It is noted that the peak wavelength of both the measured and calculated ATR spectra for different incident angles of $\theta = 56°$–$64°$ is closely matched at around 157 nm. The deviation of experimental and calculated results may be caused by the range of incident angles in the measuring beam focused on the IRE surface.

However ATR spectra are not identical to the transmittance spectra. It is known that ATR spectra include not only absorption but also refractive index. The intensity shift can be readily corrected by Eq. (2.1), but the shift in the wavelength due to the refractive index cannot be corrected. In order to separate the contributions of the absorption and refractive indices, Kramers–Kronig transformation (KKT) and Fresnel formulas should be used [19]. The experimentally observed reflectivity R

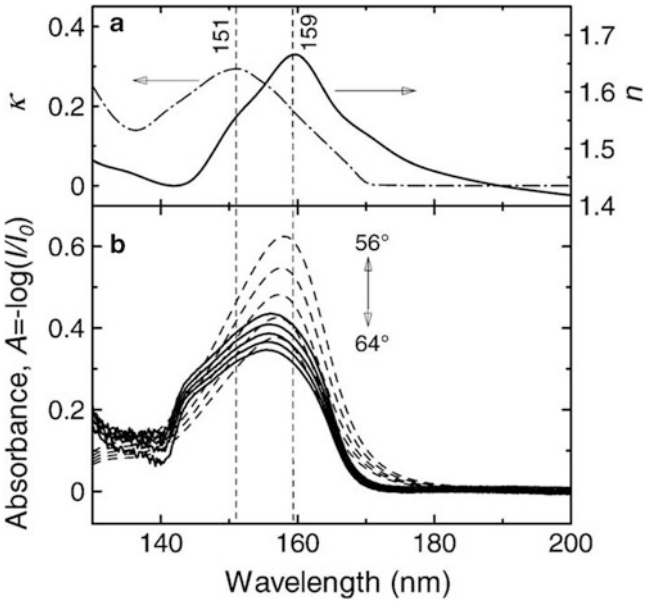

Fig. 2.5 (**a**) The refractive indices and absorption indices of water obtained by Painter et al. [17]. (**b**) *Broken* and *solid lines* show the simulated and measured ATR–FUV spectra, respectively, at a variety of incident angles

can be converted into the phase shift spectra by using KKT that can be written as a function of frequency, i.e.,

$$\Phi(v) = I - \frac{2v}{\pi}\int_0^{\infty} \frac{\ln n\sqrt{R\,(v')}}{v'^2 - v^2}dv' \tag{2.2}$$

where I is a correction term for the phase shift at a reflection surface [20]. In order to apply Eq. (2.1) to the discrete reflection data, Maclaurin's formula is adopted as an approximation [21]. The phase spectra for this case are eventually given by

$$\Phi_i = \mathrm{Arc\,tan}\left(\frac{\sqrt{n_\mathrm{p}^2\sin^2\theta - n_\infty^2}}{n_\mathrm{p}\sin\theta}\right) + \frac{2v_i}{\pi}2\,(v_{i+1} - v_i)\sum_j \frac{\ln\sqrt{R_j}}{v_j{}^2 - v_i{}^2} \tag{2.3}$$

where n_p and θ represent the refractive index of an IRE and the angle of incidence, respectively. For the sapphire IRE, we set np as 2.0. The summation is performed by taking every other data point. That is, l is odd, $m = 2, 4, 6, \ldots, l-1, l+1, \ldots,$ and when l is even, $m = 1, 3, 5, \ldots, l-1, l+1, \ldots$. According to the Fresnel reflection, amplitude reflectance is given by $r = \sqrt{R}\exp(i\,\Phi)$. The refractive index n and absorption index κ are thus calculated using the formulas

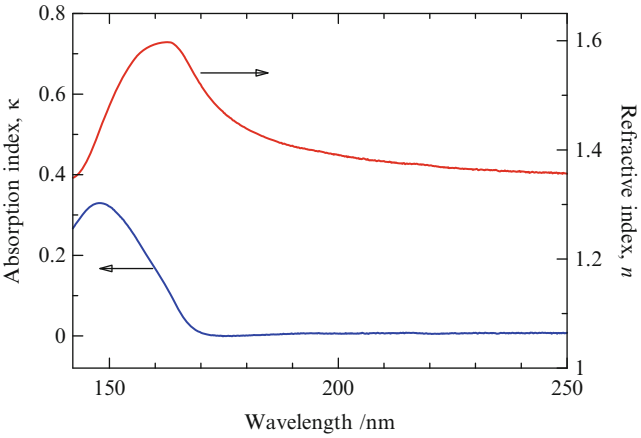

Fig. 2.6 The separated κ and n spectra of water by KKT from an ATR–FUV spectrum measured at 25 °C

$$n = n_\infty \mathrm{Re}\left[\sqrt{\sin^2\theta + \left(\frac{1-\tilde{r}}{1+\tilde{r}}\right)^2 \cos^2\theta}\right] \tag{2.4}$$

and

$$\kappa = -n_\infty \mathrm{Im}\left[\sqrt{\sin^2\theta + \left(\frac{1-\tilde{r}}{1+\tilde{r}}\right)^2 \cos^2\theta}\right], \tag{2.5}$$

where n_∞ is a refractive index of sample in the high-frequency limit. The KKT algorithm can be validated using an artificial absorption band on the basis of Lorentzian distribution. We employ the values of n_D at 589 nm instead of n_∞ for the actual case, for example, $n_\mathrm{D} = 1.333$ for water. In order to obtain the desired result, the experimental data should be probably extrapolated. In case of water absorption, the spectrum was extrapolated from 145 nm to 120 nm by nonlinear least squares fit with an ATR spectrum modeled with Gaussian line shapes based on Heller's optical constants of water [22]. Figure 2.6 shows the separated κ and n spectra of water measured at 25 °C. The absorption spectrum shows the first electronic transition peaked at 148 nm that is shorter than that found in the raw ATR spectrum. In the n spectrum, a strong dispersion is found in the FUV region of $\lambda < 163$ nm. A peak appears at around 163 nm and an anomalous dispersion is estimated below 163 nm. The property of the ATR–FUV spectra of water in different states will be detailed in Chap. 4.

The ATR–FUV spectrometer has been used for both basic research on hydrogen bonding and hydration of water and electronic transitions and structure of organic molecules such as alcohols and ketones and has been applied to qualitative and

quantitative analysis and on-line monitoring. The current trends in the development of optical devices toward the FUV region have brought us the use of high-groove density gratings, small light sources, and small detectors. Higashi et al. developed a miniaturized practical spectrometer for semiconductor manufacturing processes with a nitrogen purging system and realized the in-line monitoring of liquid chemicals in very low concentration level [23]. Of course ATR–FUV spectroscopy is useful for the measurement of solid samples. The practicability has been gradually confirmed for some polymer film sample. As will be shown in Chap. 3, Sect. 3.3.5, the cast films of nylons were measured by using an ATR–FUV spectrometer mentioned in this section. This study demonstrated that one can investigate the electronic structure and transitions of polymers on the extreme surface.

2.3 Time-Resolved ATR–FUV Spectroscopy

An FUV transient absorption spectrometer based on time-resolved (TR) ATR has developed and tested for aqueous solutions of phenol and tryptophan in the region 170–185 nm [13]. Figure 2.7 shows a schematicdiagram of the TR-ATR–FUV spectrometer. The conception of the TR-ATR–FUV is based on a nanosecond transient absorption spectrometer with an ATR–FUV sample compartment. In this region, a stable tunable laser was not available, and therefore, white light from a laser-driven Xe lamp source was used as a probe light. The probe light is incident to the IRE at an incident angle of 70°. The IRE was placed in the ATR probe. A new ATR probe where a sample liquid is exchanged continuously by a flow system was designed to reduce efficiently the stray light from the excitation light. Figure 2.8a

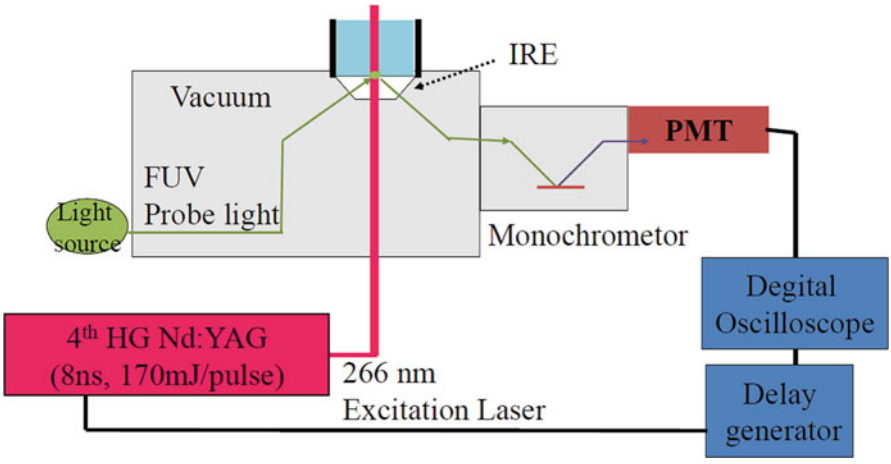

Fig. 2.7 A schematic diagram of the time-resolved attenuated total reflectance far-ultraviolet spectrometer that we developed

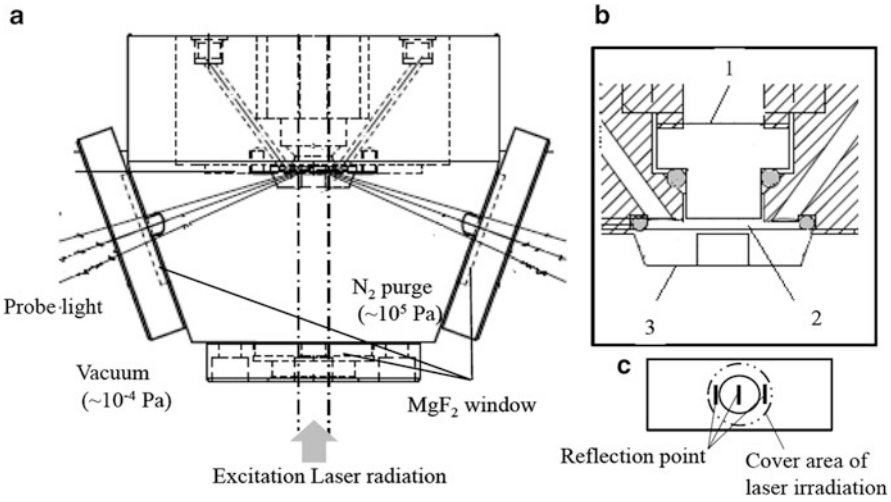

Fig. 2.8 The attenuated total reflectance probe used as part of the time-resolved attenuated total reflectance far-ultraviolet spectrometer (**a**). An enlarged figure of the internal reflection element in side view (**b**) and bottom view (**c**)

illustrates the ATR probe. The sample solution flows through the cell (Fig. 2.8b-2) at 80 ml/min. A three-time internal reflection (Fig. 2.8c) element (IRE) made of quartz is employed (Fig. 2.8b-3). Subsequent to the IRE, a monochromator is placed. A solar blind response photomultiplier (PMT; R6835, Hamamatsu Photonics) with a homemade preamplifier is used to detect the probe light. The time resolution, which was determined by the time response of a continuous light detector, was 40 ns.

We have examined the performance of the instrument by using 5×10^{-3} mol dm^{-3} phenol aqueous solution irradiated by a 266-nm laser pulse in the range of 170–185 nm. Figure 2.9 shows a temporal signalfor 172- and 181-nm probe light that was delayed by the laser irradiation. As for the signal at 172 nm, a difference signal in a unit of absorbance suddenly increases in a limit of response time, and then the signal gradually decreased. Compared to signal at 172 nm, the signal at 181 nm suddenly decreased after laser irradiation and then gradually increased. Figure 2.10 shows the transientabsorption spectra of the aqueous solution of phenol in the region 170–185 nm for various time delays. In the very short time delay, the transient absorption increased for the wavelength region that was greater than 175 nm, while the absorption signal decreased for the region that was shorter than 176 nm. The absorption at 172 nm that increased immediately after laser irradiation may have been due to the transient species created by photodissociation. On the other hand, the intensity that decreased in the longer wavelength region at 176 nm that was induced by the laser irradiation may be ascribed to the decrease in the phenol π-π^* band due to the photodissociation of phenol. Many studies on the photodissociation of phenol in aqueous solutions over various time ranges have been carried out [24, 25]. For the time range of 250 μs on which our system focuses,

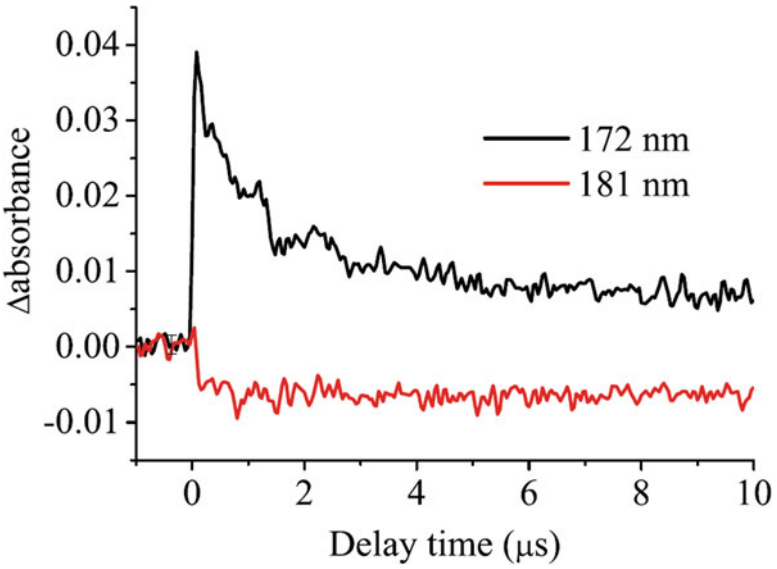

Fig. 2.9 A temporal signal for 172- and 181-nm probe light delayed from the laser irradiation

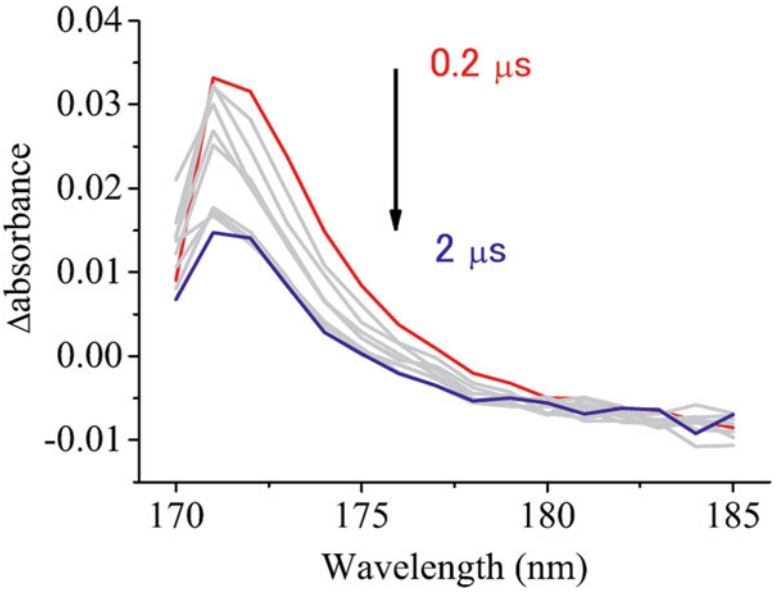

Fig. 2.10 Transient absorption spectra in the 170–185-nm region of the phenol solution (3.0×10^{-3} mol dm^{-3})

previous studies examined the time-resolved EPR, and time-resolved transient absorption spectra were measured for phenol aqueous solutions [24, 25]. With reference to these studies, we inspected the signal in Fig. 2.9 and concluded that the decrease in intensity of the phenol signal within 10 ns after laser irradiation was in good agreement with the decrease in intensity of the longer wavelength region at 177 nm.

2.4 Conclusion

FUV spectroscopy had not been widespread in the past several tens of years because of interference by the strong absorption of oxygen in air. The solution has been thought to be evacuation of the instrument; therefore the wavelength region was called vacuum ultraviolet. The nitrogen purge is the alternative approach to the FUV region and it realizes the spectral measurements under atmospheric pressure. This approach simplifies the instruments and provides possibility of transmittance measurements with a fragile cell as well as the ATR measurements. Unfortunately, there have been no innovations in the light source and detector in the FUV spectrometer explained in this chapter. For example, the photomultiplier still needs wavelength conversion with a sodium salicylic acid film. To provide a highly sensitive measurement, more stable elements should be developed. We hope that the findings by the ATR–FUV spectrometer motivate and accelerate the developments of optical elements in the FUV region.

References

1. J.-J. Max, M. Trudel, C. Chapados, Appl. Spectrosc. **52**, 234 (1998)
2. J.-J. Max, C. Chapados, Appl. Spectrosc. **52**, 963 (1998)
3. K. Masuda, T. Haramaki, S. Nakashima, B. Habert, I. Martinez, S. Kashiwabara, Appl. Spectrosc. **57**, 274 (2003)
4. N. J. Harrick, *Internal Reflection Spectroscopy Harrick* (New York, 1987)
5. A. Hartstein, J.R. Kirtley, J.C. Tsang, Phys. Rev. Lett. **45**, 201 (1980)
6. S. Morita, M. Tanaka, Y. Ozaki, Langmuir **23**, 3750 (2007)
7. L. Xu, J.R. Schlup, Appl. Spectrosc. **50**, 109 (1996)
8. A. Ikehata, X. Li, T. Itoh, Y. Ozaki, J.-H. Jiang, Appl. Phys. Lett. **83**, 2232 (2003)
9. K. Matsubara, S. Kawata, S. Minami, Appl. Spectrosc. **42**, 1375 (1988)
10. A. Pirnia, C.S.P. Sung, Macromolecules **24**, 6104 (1991)
11. W.M. Doyle, L. Tran, Spectroscopy **14**, 46 (1999). Amsterdam
12. D.R. Thompson, E. Kougoulos, A.G. Jones, M.W. Wood-Kaczmar, J. Cryst. Growth **276**, 230 (2005)
13. Y. Ozaki, Y. Morisawa, A. Ikehata, N. Higashi, Appl. Spectrosc. **66**, 1 (2012)
14. Y. Morisawa, N. Higashi, K. Takaba, N. Kariyama, T. Goto, A. Ikehata, Y. Ozaki, Rev. Sci. Instrum. **83**, 073103 (2012)
15. N. Higashi, A. Ikehata, Y. Ozaki, Rev. Sci. Instrum. **78**, 103107 (2007)
16. N.J. Harrick, Phys. Rev. Lett. **4**, 224 (1960)

17. L.R. Painter, R.D. Birkhoff, E.T. Arakawa, J. Chem. Phys. **51**, 243 (1969)
18. D.B. Leviton, T.J. Madison, P. Petrone, Proc. SPIE-Soc. Opt. Eng. **3425**, 219 (1998)
19. A. Ikehata, Y. Ozaki, N. Higashi, J. Chem. Phys. **129**, 234510 (2008)
20. J.A. Bardwell, M.J. Dignam, J. Chem. Phys. **83**, 5468 (1985)
21. K. Ohta, H. Ishida, Appl. Spectrosc. **42**, 952 (1988)
22. J.M. Heller Jr., R.N. Hamm, R.D. Birkhoff, L.R. Painter, J. Chem. Phys. **60**, 3483 (1974)
23. N. Higashi, H. Yokota, S. Hiraki, Y. Ozaki, Anal. Chem. **77**, 2272 (2005)
24. A. Bussandri, H. van Willigen, J. Phys. Chem. A **106**, 1524 (2002)
25. T.A. Gadosy, D. Shukla, L.J. Johnston, J. Phys. Chem. A **103**, 8834 (1999)